1985

SAE The Engineering Resource For Advancing Mobility

400 COMMONWEALTH DRIVE WARRENDALE, PA 15096

SAE Technical Paper Series

850047

Laminar Burning Speed Measurements of Indolene-Air-Diluent Mixtures at High Pressures and Temperatures

David B. Rhodes
Atomic Energy of Canada Limited
James C. Keck
Massachusetts Institute of Technology

International Congress
& Exposition
Detroit, Michigan
February 25 – March 1, 1985

850047

Laminar Burning Speed Measurements of Indolene-Air-Diluent Mixtures at High Pressures and Temperatures

David B. Rhodes
Atomic Energy of Canada Limited
James C. Keck
Massachusetts Institute of Technology

ABSTRACT

The laminar burning speeds of two practical multi-component hydrocarbon fuels similar to automotive gasoline were measured using a spherical combustion bomb with central ignition. Mixtures with equivalence ratios between 0.7 and 1.6, and volume fractions of simulated residual gas between 0 and 0.3 were tested at pressures from 0.4 atm to 12 atm and unburned gas temperatures from 350 K to 550 K. The laminar burning speeds were fitted to a power function expression involving the unburned gas pressure and temperature, and the diluent fraction.

The pressure and temperature dependences of the laminar burning speed for undiluted mixtures agreed well with values reported by other investigators for various fuels, indicating that these dependences are independent of fuel type. The percentage reduction in laminar burning speed due to the addition of simulated residual gas was found to be a function only of the amount added, independent of the properties of the mixture.

THE LAMINAR BURNING SPEED, or rate of flame propagation relative to the unburned gas, in practical fuel-air-residual gas mixtures is a fundamental parameter that influences the performance and emissions of internal combustion engines. It is needed in turbulent burning models (1,2,3)* which consider turbulent flames to be composed of many small pockets of unburned gas, each of which is surrounded by a laminar flame. The laminar burning speed also affects the quench layer thickness (4,5), ignition limits, ignition energy, and ignition delay of a mixture.

Some investigators (6,7,8,9) have attempted to model the propagation of laminar flames by considering the elementary reactions that take place in the flame and the mass and thermal diffusivities of the various species. This procedure is very complicated for pure fuels, and has not been attempted for practical multi-component fuels.

In this study, the laminar burning speeds of two multi-component fuels similar to automotive gasoline mixed with air and simulated residual gas are measured for a wide range of equivalence ratios. The simulated residual gas is composed of 80% N_2 and 20% CO_2 by volume. It was chosen to match the heat capacity of the actual exhaust products from stoichiometric combustion of the fuels tested.

Tests are made in a spherical combustion bomb with central ignition. The main advantage of the combustion bomb technique over others is that, because the unburned gas is compressed as the mixture burns, data is obtained for a wide range of temperatures and pressures from a single run. Laminar burning speeds are calculated from the pressure history by first solving for the mass burning rate required to give the observed rate of pressure rise, and then dividing this by the calculated density of the burned gas and the flame area.

$$S_u = \frac{\dot{m}}{A_f \rho_u} \qquad (1)$$

where:

S_u = laminar burning speed
$\dot{m}$ = mass burning rate
A_f = area of the flame front
ρ_u = density of the unburned gas

Metghalchi and Keck (10,11) have used the same facility to measure burning speeds of mixtures of air with propane, methanol, isooctane, and RMFD 303 (which is one of the multi-component fuels tested in this study) for equivalence ratios of 0.8, 1.0, and 1.2. Ryan and Lestz (12) have used a similar combustion bomb to investigate the effect of diluent on the laminar burning speeds of five pure fuels. The results of these

*Numbers in parentheses designate references at the end of the paper.

0148-7191/85/0225-0047$02.50

other combustion bomb studies and the predictions of the theoretical models mentioned earlier compare favorably with our results.

EXPERIMENTAL APPARATUS AND PROCEDURE

COMBUSTION BOMB - The facility used in this study is described in Reference (10). The spherical combustion bomb is shown in Figure 1. Mixtures are ignited using a capacitive discharge system and two electrodes which extend to the centre of the bomb. The bomb is contained in an oven heated by eight 250 W resistance heaters mounted on the oven wall and by one 1400 W resistance heater wrapped around the flanges of the bomb. The temperature throughout the oven and on the outer surface of the bomb is measured using four thermocouples and is kept uniform by a fan mounted at the top of the oven.

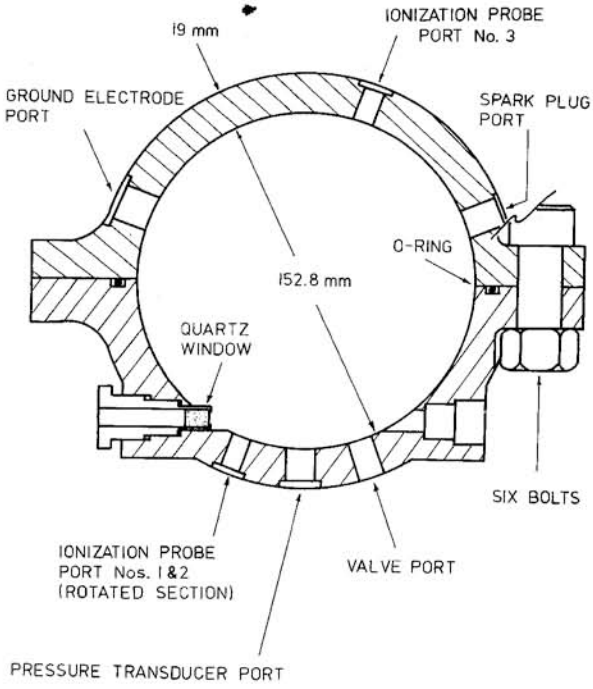

FIGURE 1: Combustion bomb.

A schematic of the gas and fuel handling system is shown in Figure 2. Bourdon tube gauges of various ranges are used to measure gas pressures, and thermocouple gauges are used to measure vacuum pressure. To ensure that the N_2-CO_2 mixture used to simulate the effect of exhaust gas recirculation is the same for all shots, and to simplify the charging process, a large supply of diluent is premixed in the storage reservoir.

To prepare for a run, the bomb is evacuated and then the required volume of liquid fuel is injected through a silicone septum using a gas-tight syringe. The desired pressure of fuel vapour is calculated from the ideal gas law and is then checked using the balanced pressure indicator described in the Appendix. To prevent

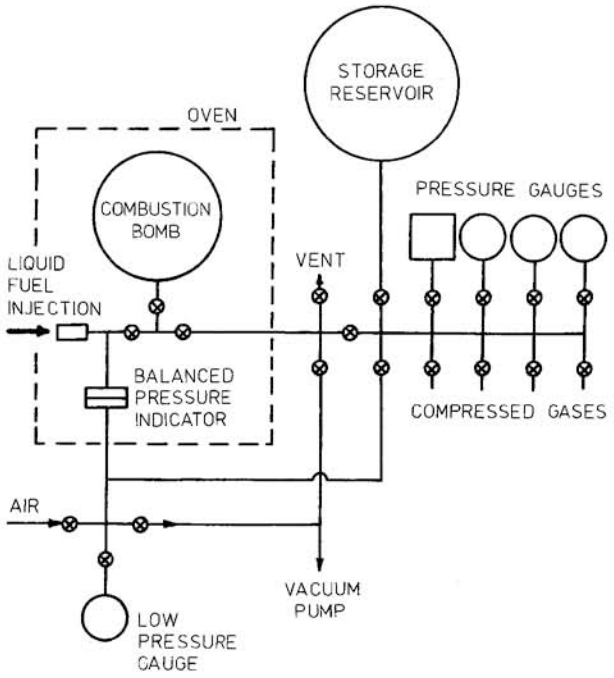

FIGURE 2: Gas and fuel handling system.

the heavier fractions of the multicomponent fuels tested in this study from condensing, the fuel must be completely contained in the heated oven. The balanced pressure indicator, which is located inside the oven, isolates the fuel from a balancing pressure which is applied from the outside. The balancing pressure is adjusted until it equals the fuel pressure and is measured using a bourdon gauge. The required pressures of diluent and air are then added. To ensure that the gas in the bomb is at rest, it is left to sit for five minutes before it is ignited.

INSTRUMENTATION - A schematic of the three main instrumentation systems is shown in Figure 3. The principal instrumentation on the combustion bomb is the pressure measuring system. It consists of a Kistler model 603B1 piezoelectric transducer (coated with a 0.5 mm layer of high vacuum grease to reduce thermal sensitivity) and a model 504A charge amplifier connected to an ADAC System 1000 microprocessor and an oscilloscope equipped with a Polaroid

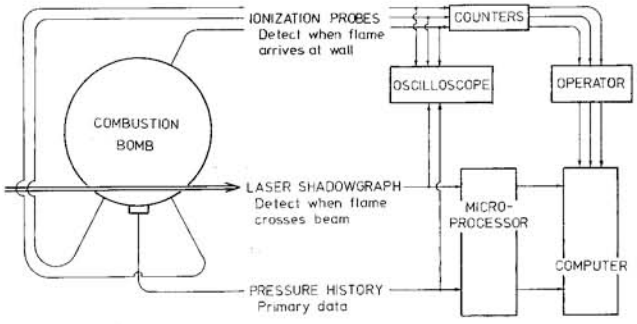

FIGURE 3: Schematic of data acquisition system.

camera. The pressure signal is digitized and stored temporarily by the microprocessor, and then transferred to a PDP-11/60 computer for analysis.

The ionization probes determine the arrival times of the flame at three points on the wall and are used to check whether or not the flame was actually symmetrical about the centre of the bomb. They consist of a copper insulated electrode inside a stainless steel body. When the flame arrives at an ionization probe, the gas between the end of the electrode and the body becomes conductive and permits a capacitor to discharge. A sharp pulse is produced which stops a counter and is recorded by the oscilloscope. The ionization probe times are then input into the computer by the operator.

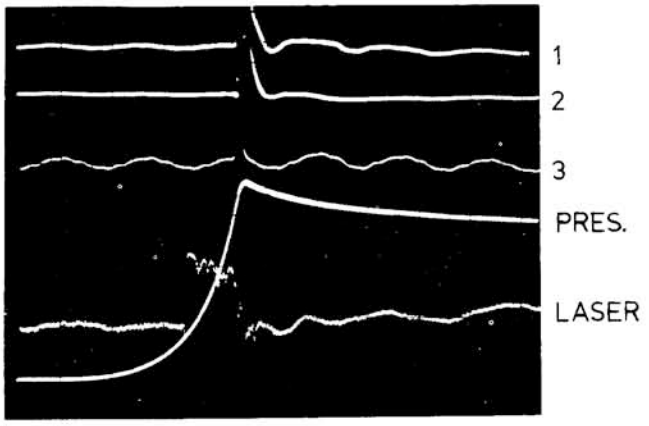

FIGURE 4: Typical oscillogram showing the three ionization probe signals (1 - bottom left, 2 - bottom right, 3 - top), as well as the pressure and laser signals. RMFD 303, ϕ=1.4, p_i=2 atm, T_i=350 K, 10 ms/division sweep rate.

The laser shadowgraph system determines the time at which the flame reaches a known radius. The laser signal is recorded by both the oscilloscope and the microprocessor. The data analysis program then compares its calculated flame position at this time with the known position of the laser beam.

A typical oscillogram showing pressure, ionization probe, and laser signals is shown in Figure 4. The following section describes the procedure used to analyze this data.

ANALYSIS OF DATA

CALCULATION OF LAMINAR BURNING SPEED FROM THE PRESSURE HISTORY - The combustion process in a spherical combustion bomb with central ignition can be modelled as an unsteady one-dimensional problem by assuming that all parameters are only a function of radial distance from the centre of the bomb. A further simplification is made here by recognizing that the unburned gas is all at one state and by assuming that the burned gas is all at another. This unsteady lumped-parameter model eliminates the need for spatial integration.

The method used in this study to calculate the laminar burning speed from the pressure history is also discussed by Metghalchi and Keck (11). The basic assumptions made are:

1. There is no stratification of the charge.
2. The flame front is smooth and spherical.
3. The thickness of the flame front is negligible.
4. The pressure at any given time is constant throughout the bomb.
5. There are no preflame reactions in the unburned gas.
6. The burned gas is in thermodynamic equilibrium. Burned gas properties are calculated using the equilibrium program of Martin and Heywood (13).
7. There is no heat transfer between gas elements in the bomb, except in a thermal boundary layer in the unburned gas next to the bomb wall.
8. An element of unburned gas is first compressed isentropically, then is burned in a constant enthalpy and constant pressure process, and finally is compressed isentropically to its final state.

Based on these assumptions, the volume and energy balance equations for the gas in the bomb are:

$$\frac{V}{M} + \frac{A\delta}{M} = \int_0^x v_b dx' + \int_x^l v_u dx' \qquad (2)$$

$$\frac{E}{M} - \frac{A}{M}\int_0^\delta p d\delta' = \int_0^x e_b dx + \int_x^l e_u dx' \qquad (3)$$

where:

V = volume of the combustion bomb
M = mass of the gas in the bomb
A = area of the bomb wall
E = initial internal energy of the gas in the bomb
δ = thermal boundary layer displacement thickness of the unburned gas next to the bomb wall, discussed in Reference (14)
v = specific volume
e = specific internal energy
x = mass fraction burned

and the subscripts b and u refer to the burned and unburned gas respectively.

The unburned gas is compressed isentropically from a uniform initial state, so at any subsequent time the state of the unburned gas is still uniform:

$$v_u = v_u(p, s_{uo}) \qquad (4)$$

$$e_u = e_u(p, s_{uo}) \qquad (5)$$

where s_{uo} is the initial specific entropy of the gas in the bomb.

The burned gas is not all at the same state, though, because the increase in entropy of gas elements as they burn changes as combustion proceeds. Thus, gases burned at different times are compressed along different isentropes. The specific volume and internal energy of an element of burned gas can be expressed as:

$$v_b = v_b(p,\bar{T}_b) + \left(\frac{\partial v_b}{\partial T}\right)_p\Big|_{\bar{T}_b}(T - \bar{T}_b) + \frac{1}{2}\left(\frac{\partial^2 v_b}{\partial T^2}\right)_p\Big|_{\bar{T}_b}(T - \bar{T}_b)^2 + \cdots \quad (6)$$

$$e_b = e_b(p,\bar{T}_b) + \left(\frac{\partial e_b}{\partial T}\right)_p\Big|_{\bar{T}_b}(T - \bar{T}_b) + \frac{1}{2}\left(\frac{\partial^2 e_b}{\partial T^2}\right)_p\Big|_{\bar{T}_b}(T - \bar{T}_b)^2 + \cdots \quad (7)$$

where $\bar{T}_b$ is the mass average temperature of the burned gas.

$$\bar{T}_b = \frac{1}{x}\int_0^x T\,dx' \quad (8)$$

The first order terms of Eqs. (6) and (7) vanish when these expressions are substituted into Eqs. (2) and (3). For an ideal gas with constant specific heats, the second order terms would be identically zero, but since the composition and specific heats of the burned gas change slightly with temperature, these terms are not identically zero for our case. The volume and energy balance equations thus simplify to:

$$\frac{V}{M} + \frac{A\delta}{M} = xv_b(p,\bar{T}_b) + (1-x)v_u(p,s_{uo}) + O\left(\left(\frac{\partial^2 v_b}{\partial T^2}\right)_p\Big|_{\bar{T}_b}\overline{(T - \bar{T}_b)^2}\right) \quad (9)$$

$$\frac{E}{M} - \frac{A}{M}\int_0^\delta p\,d\delta' = xe_b(p,\bar{T}_b) + (1-x)e_u(p,s_{uo}) + O\left(\left(\frac{\partial^2 e_b}{\partial T^2}\right)_p\Big|_{\bar{T}_b}\overline{(T - \bar{T}_b)^2}\right) \quad (10)$$

This is a set of simultaneous equations with unknowns $\bar{T}_b$ and x. Metghalchi has shown that the error in the calculated value of x is negligible when the second order terms are dropped. Thus, the combustion process is broken into steps and Eqs. (9) and (10), without the second order terms, are solved iteratively for the current values of $\bar{T}_b$ and x at each step. Knowing the mass fraction burned and specific volumes of the burned and unburned gases, the flame position and laminar burning speed, S_u, is calculated as follows:

V_b = volume of the burned gas sphere

$$= Mxv_b(p,\bar{T}_b) \quad (11)$$

r = radius of the flame front

$$= \left(\frac{3}{4\pi}V_b\right)^{1/3} \quad (12)$$

A_f = area of the flame front

$$= 4\pi r^2 \quad (13)$$

$$S_u = \frac{M\dot{x}(t)}{A_f/v_u} \quad (14)$$

Instead of calculating $\dot{x}(t)$ by numerically differentiating the calculated values of $\dot{x}(t)$, the pressure history is numerically differentiated to find $\dot{p}(t)$. To reduce errors caused by round-off in the microprocessor and by signal noise, the pressure data is locally smoothed over each of about 15 burning steps and then x is calculated at each burning step using the relation

$$\dot{x} = \frac{dx}{dp}\dot{p} \quad (15)$$

where dp/dx is obtained by differentiating Eq. (9):

$$\frac{dx}{dp} = \frac{v_i\left[1 - (1-x)\frac{v_u}{v_i}\left(1 - \frac{\gamma_b}{\gamma_u}\right) + \frac{A}{V}\left(\gamma_b p\frac{d\delta}{dp} + \delta\right)\right]}{\gamma_b(R_b T_b^\circ - R_u T_u)} \quad (16)$$

v_i = initial specific volume of the mixture

γ = specific heat ratio

R = gas constant

T_b° = adiabatic flame temperature

As stated earlier, a number of basic assumptions are made in deriving the above expressions. The errors introduced by these assumptions are not expected to be over 1%. In subsequent sections, two phenomena not accounted for in either the analysis or the basic assumptions are discussed.

HEAT TRANSFER TO THE ELECTRODES - Although the data analysis program accounts for the heat

transferred from the unburned gas to the bomb wall; it assumes that the heat transfer from the much hotter burned gas to the electrodes is negligible. To test the validity of this assumption, the thickness of the thermal boundary layer around the electrodes was first calculated assuming pure conduction. Since the thermal mass of the electrodes is of the same order of magnitude as the thermal mass of the gas inside the bomb, the temperature of the electrodes was assumed to remain constant. For a stoichiometric RMFD 303 run with no diluent and an initial pressure and temperature of 1 atm and 350 K, only about 0.1% of the total gas in the bomb would be contained in the thermal boundary layers around the electrodes.

Actually though, the burned gas is not stationary; the most recently burned gas moves toward the centre of the bomb with a speed of the same order of magnitude as the laminar burning speed. Since this unsteady convection problem is difficult to analyze theoretically, it was approached experimentally. Two dummy electrodes were inserted into the bomb and then four identical propane runs were made (ϕ = 1.0, p_i = 1 atm T_i = 350 K). There was no observable difference between these runs and similar runs made without the dummy electrodes, so heat transfer to the electrodes was concluded to have a negligible effect on the calculated burning speed.

BUOYANCY - Since the density of the hot burned gas is only about one fifth that of the unburned gas, the burned gas sphere tends to rise towards the top of the bomb. For slow runs, where buoyancy has time to become significant, the time of arrival of the flame front at the top ionization probe is earlier than the times of arrival at the bottom probes. For such runs, the laser shadowgraph signal indicates that the flame arrived at the beam later than expected. In this study, buoyancy was noticeable for runs where the minimum measured flame speed was less than about 25 cm/s and became severe when the minimum measured flame speed was less than about 12 cm/s (which only occurred for diluent fractions of 0.25 and 0.3).

Figure 5 shows the effect of buoyancy on the pressure history. In runs where buoyancy is significant, the time at which the flame arrives at the top wall coincides with an inflection point in the pressure curve. After the flame reaches the wall, there is significant heat loss from the burned gas to the wall. Normally, the heat loss is immaterial because the combustion process has finished, but in runs where the burned gas rises, heat is lost before all of the gas has burned. This slows the rate of rise of pressure, and reduces the maximum pressure. Also, after the flame front reaches the top wall, the area of the front decreases drastically. This decrease reduces the rate at which gas is burned, which in turn reduces $\dot{p}$. The data analysis program calculates laminar burning speeds assuming that the flame front is spherical and that there is no heat loss from the burned gas to the wall, so the calculated speeds after the inflection time are much too low, and are not used.

To obtain a qualitative understanding of the buoyancy problem, an approximate analytical model was developed. It was found that the significant factors controlling the buoyant rise of the burned gas are:

1. The gas is contained in a closed vessel.
2. The burned gas sphere is expanding faster than it consumes the unburned gas. Thus, unburned gas is being pushed ahead of the flame front.
3. Unburned gas is continually being engulfed by the flame.
4. The viscosity of the burned gas is roughly 30 times the viscosity of the unburned gas, so the burned gas can be considered to be a rigid sphere.

The fact that this phemonenon takes place in a closed vessel rather than in an infinite medium drastically reduces the buoyant rise distances because the unburned gas must be squeezed out from between the rising burned gas and the upper wall. This increases the equivalent inertia of the rising sphere and so its upward acceleration is slowed. Unburned gas is also squeezed out of the upper part of the bomb as the burned gas sphere expands while positioned off-centre in the bomb. For runs with significant buoyancy, the speed of the unburned gas being squeezed out from the top of the bomb is calculated to be of the same order of magnitude as the laminar burning speed. However, since the viscosity of the burned gas is so much greater than that of the unburned gas, it is not expected that flow parallel to the flame front will distort the front significantly.

The viscous drag between the burned and unburned gases is higher than the drag between a fluid and a solid sphere because the flame is continually removing low momentum fluid from the unburned gas flowing parallel to the flame. This increases the velocity gradient in the unburned gas, and so the shearing force is also increased.

The approximate model predicted buoyant rise distances that were two to three times greater than the observed distances. This discrepancy is due to simplifying assumptions that were made to model the flow of the unburned gas.

CALIBRATION OF THE PRESSURE SIGNAL - Due to temperature sensitivity of the piezoelectric pressure transducer, the pressure signal must be calibrated before being analyzed. Exact calibration by adjusting the sensitivity of the charge amplifier is very difficult, but an analysis of the combustion products by Sellnau (15) indicates that at least 99% of the original mixture is burned. Therefore, the pressure signal is calibrated by forcing the calculated final mass fraction of the mixture that has burned to an expected value. Assuming that the pressure rise is proportional to the mass

fraction burned, the calibrated pressure becomes

$$p(t) = p_i + \frac{x_d}{x_f}\left[p(t)_{measured} - p_i\right] \qquad (17)$$

where:

x_f = final mass fraction burned calculated using the peak pressure measured by the piezoelectric transducer

x_d = expected final mass fraction burned

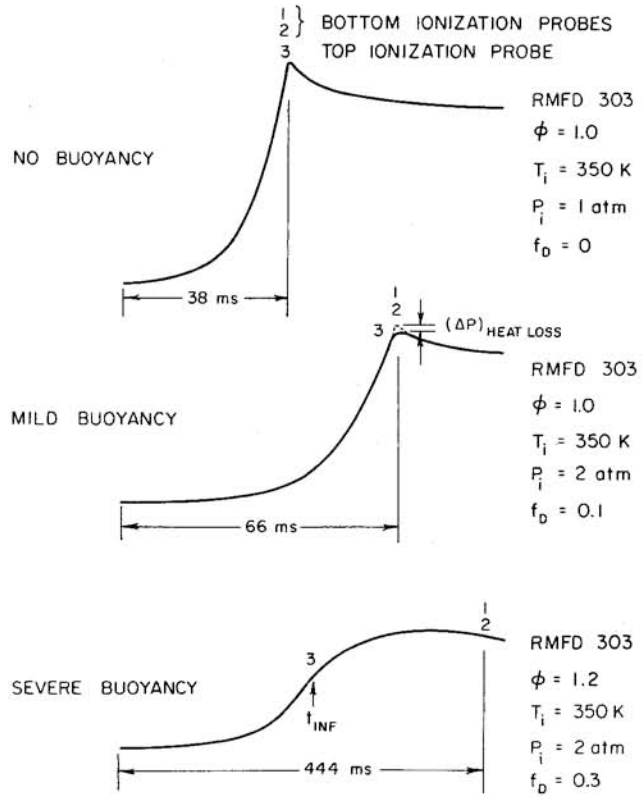

FIGURE 5: Effect of buoyancy on the pressure history. Actual pressure data and the times of arrival of the flame front at the ionization probes are shown for three typical runs.

For runs where buoyancy is not significant, x_d is chosen to be 0.99. For those runs which the peak pressure has been reduced by buoyancy, x_d is chosen by extrapolating the pressure curve upwards, as if there were no inflection point. This is shown by the dotted line on the mild buoyancy plot in Figure 5.

$$x_d = 0.99 - \frac{(\Delta p)_{heat\ loss}}{p_{max}} \qquad (18)$$

For severe buoyancy runs, the measured pressures are multiplied by a factor:

$$p(t) = p_i + C\left[p(t)_{measured} - p_i\right] \qquad (19)$$

where C is set equal to a typical value of x_d/x_f for non-buoyancy runs.

RESULTS

Laminar burning speed was measured for mixtures of air and inert gas diluent with two multi-component hydrocarbon fuels similar to

Table 1. Fuel Properties

	RMFD 302	RMFD 303
Stoichiometric Fuel/Air Ratio	0.07007	0.06988
Motor Octane Rating	80.8	88.3
Research Octane Rating	91.0	101.4
Density (kg/m^3)	749	765
Average Molecular Formula	$C_{8.056}H_{15.121}$	$C_{7.8}H_{12.214}$
Average Molecular Weight	111.9	106.9
Distillation Curve (K)		
Initial Boiling Point	305	304
50%	384	385
End Point	458	451

Manufacturer: Howell Hydorcarbons, San Antonio, Texas

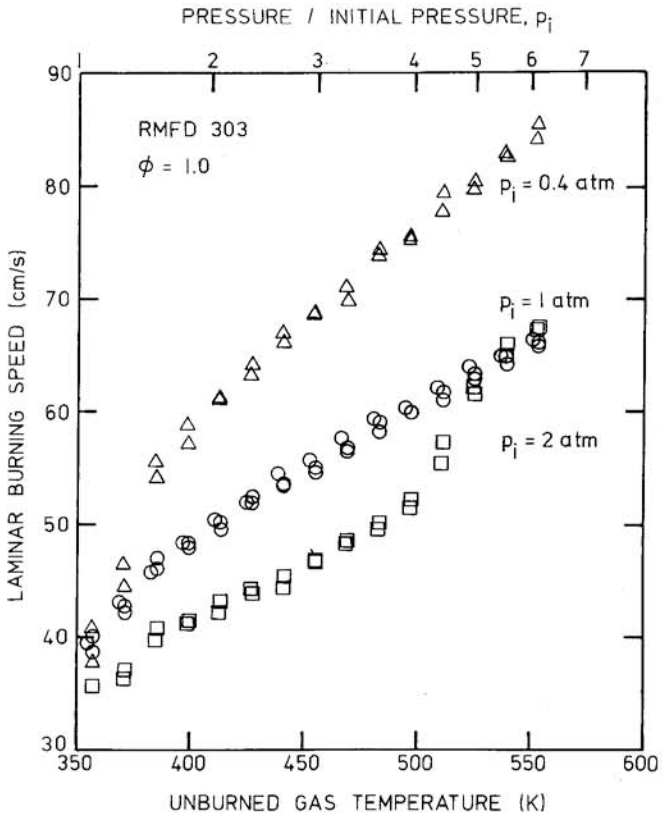

FIGURE 6: Reproducibility of laminar burning speed data for undiluted stoichiometric RMFD 303-air mixtures starting at three different initial pressures (p_i).

automotive gasoline. The Research Octane Ratings of the two fuels used, RMFD 302 and RMFD 303, are 91.0 and 101.4, respectively. Other properties are listed in Table 1. All runs had an initial temperature of 350 K, which results in a final temperature of about 550 K.

UNDILUTED MIXTURES - Mixtures of RMFD 303 with equivalence rations between 0.7 and 1.6, and initial pressures of 0.4, 1, and 2 atm were tested. To avoid random errors, two runs were made for most combinations of the above initial conditions. Very few discrepancies appeared. Reproducibility of laminar burning speed data is illustrated by Figure 6, which shows S_u as a function of the pressure and the unburned gas temperature for the seven stoichiometric RMFD 303 runs that were made.

Figure 7 contains similar plots for all of the undiluted RMFD 303-air mixturex tested. Since the unburned gas is assumed to be compressed isentropically, the ratio of the pressure at any time during the combustion process to the initial pressure is a function of the unburned gas temperature, T_u, and the specific heat ratio, γ :

$$\frac{p}{p_i} = \left(\frac{T_u}{T_i}\right)^{\gamma/(\gamma-1)} \qquad (20)$$

where i refers to the initial state of the mixture. Since the specific heat ratio of the unburned gas varies slightly with equivalence ratio, the pressure scales of these plots are not exactly the same.

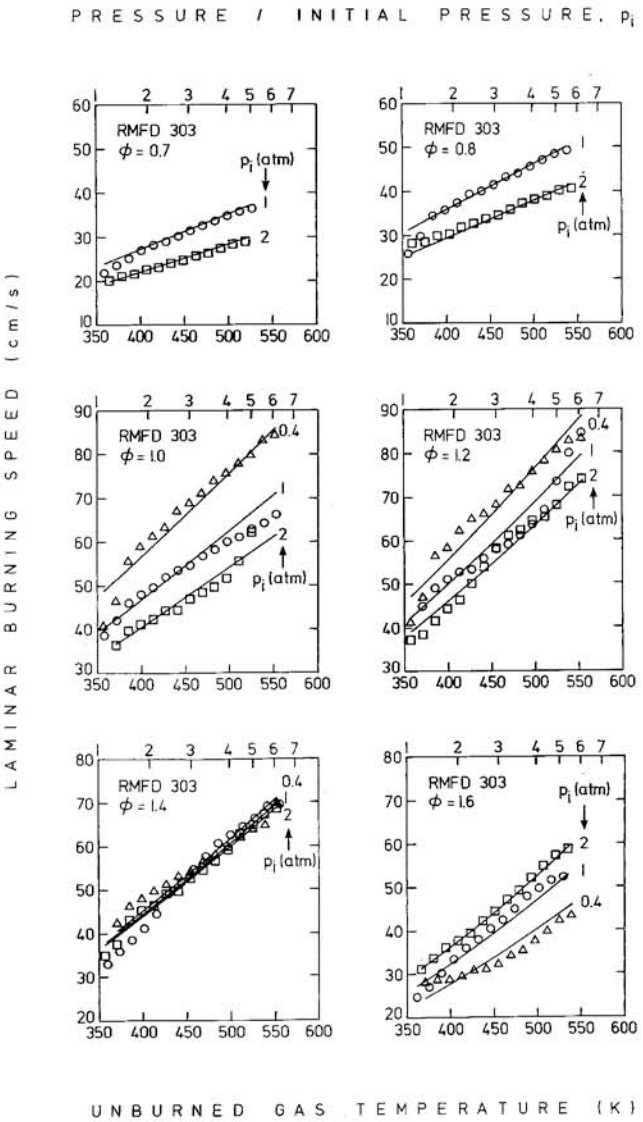

FIGURE 7: Laminar burning speed of undiluted RMFD 303-air mixtures as a function of pressure and unburned gas temperature.

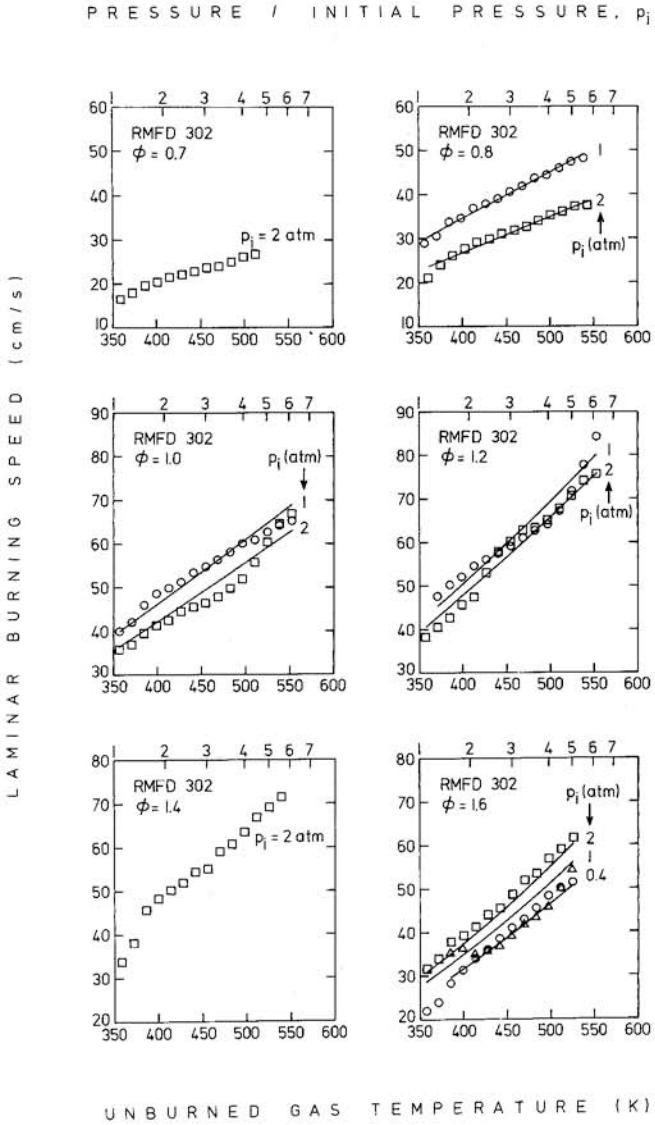

FIGURE 8: Laminar burning speed of undiluted RMFD 302-air mixtures as a function of pressure and unburned gas temperature.

Less extensive testing was done with RMFD 302-air mixtures. The plots of S_u as a function of pressure and unburned gas temperature for these mixtures are contained in Figure 8.

Very small amounts of soot were present on the bomb walls after burning mixtures of either fuel with equivalence ratios of 1.6 and 1.8, but not after burning mixtures with equivalence ratios of 1.2 or less. It was not determined whether or not soot was formed at equivalence ratios of 1.4.

DILUTED MIXTURES - RMFD 303-air mixtures were diluted with simulated residual gas, consisting of 20% CO_2 and 80% N_2 by volume. This diluent composition was chosen to match the heat capacity between 300 K and 3000 K of the actual residual gases from stoichiometric RMFD 303-air combustion. Mixtures with equivalence ratios of 0.7, 0.8, 1.0, and 1.2 were tested at an initial pressure of 2 atm and volume fractions of diluent, f_D, ranging from 0 to 0.3. Equivalence ratios of 1.0 and 1.2 were also tested at an initial pressure of 1 atm. Since the specific heat ratio, γ, of the unburned gas varies only slightly with the addition of diluent, the unburned gas is compressed along essentially the same isentrope regardless of the diluent fraction. The values of S_u obtained from all the runs made with diluent have been divided by the values of S_u for undiluted mixtures at the same pressure, unburned gas temperature, and equivalence ratio. These ratios are plotted as functions of pressure and T_u in Figure 9. The fractional reduction in laminar burning speed due to the addition of a given amount of diluent is independent of both unburned gas temperature and pressure. The average of the laminar burning speed ratios for each run in Figure 9 is plotted in Figure 10. It is apparent that the fractional reduction in S_u due to the addition of diluent is also independent of equivalence ratio.

No sooting was observed for the diluted mixtures tested.

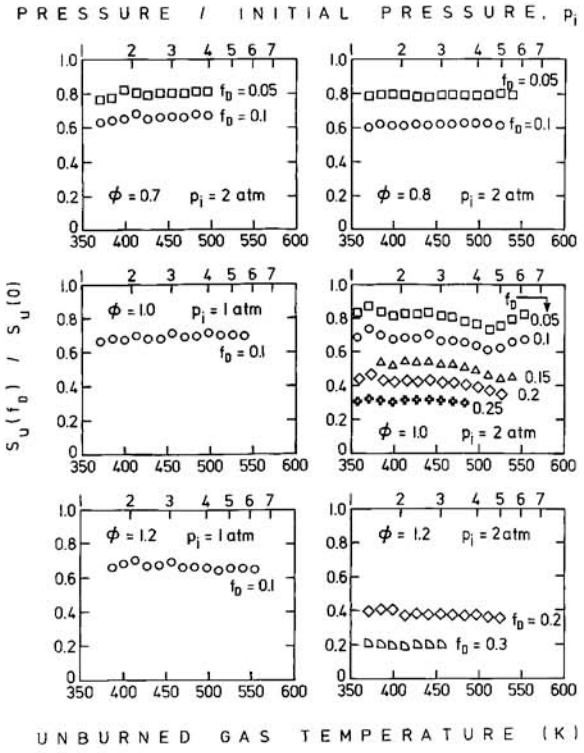

FIGURE 9: Ratio of S_u data from diluted RMFD 303-air mixtures to S_u data from the corresponding undiluted mixtures as a function of pressure and unburned gas temperature.

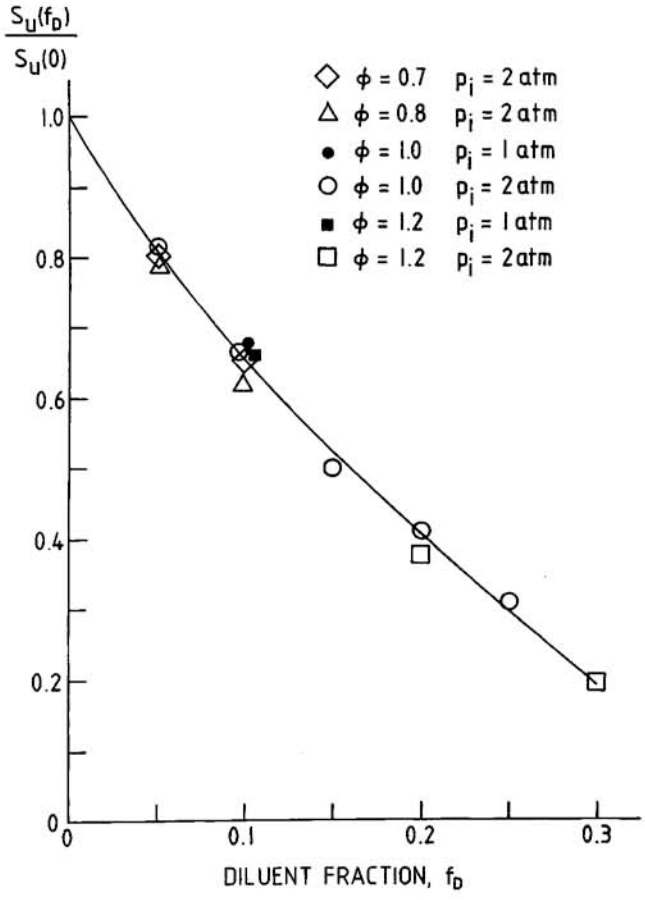

FIGURE 10: Fractional reduction in laminar burning speed as a function of diluent fraction.

CORRELATION OF DATA - The laminar burning speed data was fitted to expressions of the form

$$S_u = S_{uo} \left(\frac{T_u}{T_o}\right)^{\alpha} \left(\frac{p}{p_o}\right)^{\beta} (1 - af_D^b) \qquad (21)$$

where:

T_o = reference temperature (298 K)
p_o = reference pressure (1 atm)
T_u = unburned gas temperature
p = pressure of the gas in the bomb
f_D = volume fraction of diluent

and S_{uo}, α, β, a, and b are fitted coefficients. S_{uo}, α, and β (which are functions only of fuel type and equivalence ratio) were first evaluated for each equivalence ratio by fitting the data from a set of undiluted runs with the same equivalence ratio and different initial pressures to Eq. (21). (The diluent term drops out for $f_D = 0$.) The values of S_{uo}, α, and β for RMFD 302 and RMFD 303 are listed in Table 2 and plotted in Figure 11. The resulting fitted curves for laminar burning speed are shown in Figures 7 and 8. S_{uo}, α, and β were not evaluated for equivalence ratios for which only one run was made because the unburned gas is compressed along an isentrope and so the pressure and temperature are not independent parameters.

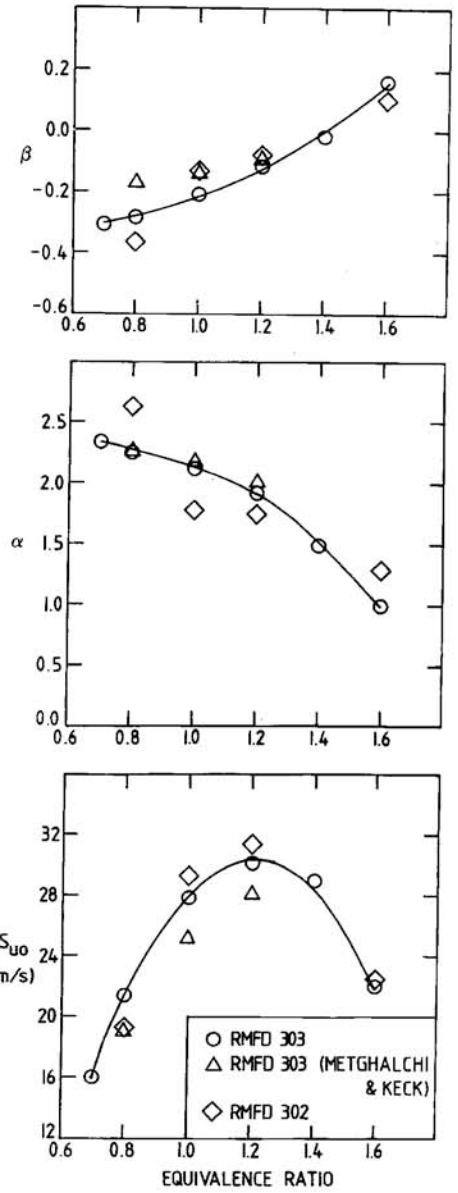

FIGURE 11: Parameters S_{uo}, α, and β, for undiluted mixtures of air with RMFD 303 and RMFD 302 as a function of equivalence ratio.

Table 2. Fitted Coefficients S_{uo}, α, and β for Undiluted Mixtures of Air with RMFD 303 and RMFD 302.

$$S_u = S_{uo}\left(\frac{T_u}{T_o}\right)^{\alpha}\left(\frac{p}{p_o}\right)^{\beta}$$

where: $T_o = 298$ K
$p_o = 1$ atm

Fuel	ϕ	S_{uo} (cm/sec)	α	β
RMFD 303	0.7	16.0	2.34	-0.308
RMFD 303	0.8	21.4	2.25	-0.284
RMFD 302	0.8	19.3	2.63	-0.367
RMFD 303	1.0	27.9	2.12	-0.208
RMFD 302	1.0	29.3	1.78	-0.131
RMFD 303	1.2	30.1	1.92	-0.116
RMFD 302	1.2	31.4	1.75	-0.077
RMFD 303	1.4	29.0	1.49	-0.019
RMFD 303	1.6	22.0	0.995	0.165
RMFD 302	1.6	22.5	1.29	0.104

Our RMFD 303 coefficients were then fitted to the following functions of equivalence ratio, ϕ:

$$S_{uo} = 30.5 - 54.9(\phi - 1.21)^2 \quad (22)$$

$$\alpha = 2.4 - 0.271\ \phi^{3.51} \quad (23)$$

$$\beta = -0.357 + 0.14\ \phi^{2.77} \quad (24)$$

The RMFD 302 coefficients were not fitted to similar expressions because they are based on less data and because they are not significantly different from the RMFD 303 coefficients. The pressure exponent, β, changes sign at $\phi = 1.4$. Figure 7 shows that at a given temperature, S_u decreases with increasing pressure for $\phi < 1.4$, S_u is a function only of T_u for $\phi = 1.4$, and S_u increases with increasing pressure for $\phi = 1.6$.

As mentioned in the previous section, the fractional reduction in S_u due to the addition of diluent is independent of equivalence ratio, pressure and temperature. Thus the parameters a and b in Eq. (21) are constant. They were evaluated for RMFD 303 by fitting the points in Figure 10 to the expression

$$\frac{S_u(f_D)}{S_u(0)} = 1 - af_D^b \quad (25)$$

The resulting values were a = 2.06 and b = 0.773.

DISCUSSION

COMPARISON WITH PREVIOUS MEASUREMENTS - The values of S_{uo}, α, and β obtained for RMFD 303 by Metghalchi and Keck (11) for equivalence ratios of 0.8, 1.0 and 1.2 are shown along with our coefficients in Figure 11. The temperature exponent, α, agrees well, but the values of S_{uo} reported in this study are about 10% higher than those reported in (11) and the pressure exponents are more negative than those in (11). The actual flame speed data for these runs with initial temperatures of 350 K agree well. The reason for the differences in S_{uo} and β is that the coefficients in (11) are also based on tests at higher pressures and temperatures.

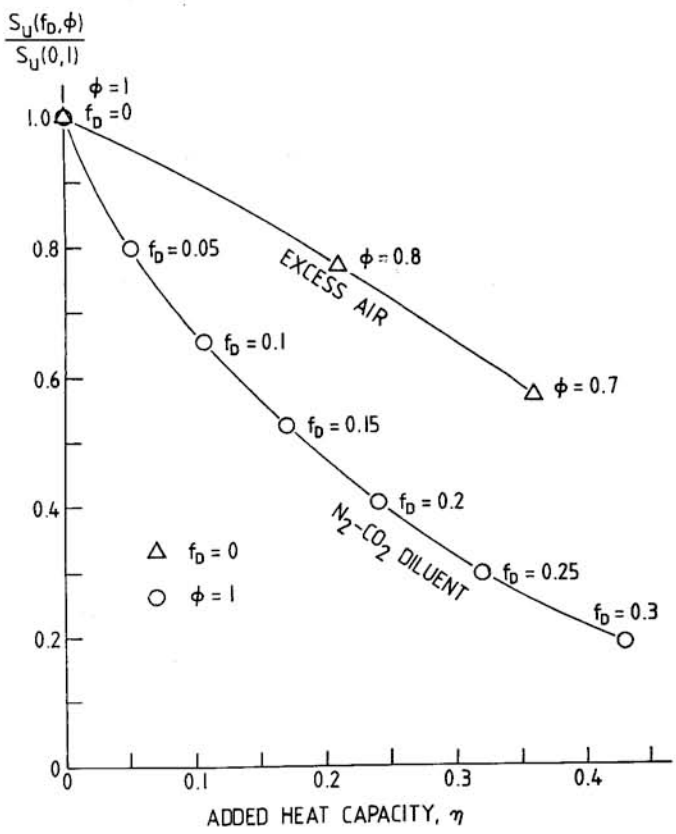

FIGURE 12: Reduction in the laminar burning speed of a stoichiometric RMFD 303-air mixture due to the addition of various amounts of excess air or N_2-CO_2 diluent.

Ryan and Lestz (12) fitted their laminar burning speed data for isooctane, n-heptane, methanol, and propane to an expression of the form

$$S_u = b_1 (p_u)^{b_2} \exp(-b_3/T_u) \quad (26)$$

where p_u is the pressure of the unburned gas and b_1, b_2, and b_3 are their fitted coefficients. Theoretically, their coefficient b_2 should correspond to our β. However, b_1, b_2, and b_3 are only obtained from one run and so the temperature and pressure dependence cannot be determined separately. They recognize this and do not recommend that their correlation be used to extrapolate S_u for conditions other than those which they tested.

Metghalchi and Keck (11) tested two stoichiometric isooctane-air mixtures with an initial pressure of 1 atm diluted with a simulated residual gas composed of 85% N_2 and 15% CO_2 by volume. This diluent has less CO_2 than ours because isooctane has a lower carbon to hydrogen ratio than RMFD 303. Metghalchi and Keck found that the addition of 10% diluent (by mass) reduced S_u by 20%, and 20% diluent reduced S_u by 40%. For 10% and 20% diluent fractions (by volume), our RMFD 303 burning speeds were reduced by 35% and 59%.

The average molecular weight of 85% N_2 - 15% CO_2 is very close to that of the unburned mixture, so the fractions of diluent by volume and mass are equal. For our diluent, the fraction by volume is 3% lower than the fraction by mass. The molal specific heat of 80% N_2 - 20% CO_2 is 3% greater than that of 85% N_2 - 15% CO_2.

Ryan and Lestz tested mixtures of isooctane, n-heptane, methanol, methane, and propane with $0.7 \leq \phi \leq 1.3$ and $0 \leq (f_D)_{mass} \leq 0.3$; however they only reported the results of their stoichiometric tests. Their diluent was 85% N_2 - 15% CO_2 by volume. For $\phi = 1.0$, $T_u = 520$ K, and $p = 6$ atm, the laminar burning speeds of the above fuels were reduced by factors similar to those given by our correlation with the average difference between their $S_u(f_D)/S_u(0)$ data and the correlation being approximately 0.04.

COMPARISON WITH THEORY - Recently, theoretical models of premixed laminar flame propagation have been developed which consider many elementary reactions and intermediate species, plus the mass and thermal diffusivities of the gases. Heimeri and Coffee (6) model ozone flames, Smoot et al. (7) and Tsatsaronis (8) model methane-air flames, and Westbrook and Dryer (9) model methanol-air flames. Westbrook and Dryer, and Tsatsaronis both fit their predicted burning speeds to expressions similar to the correlation used here. Instead of using a single expression which includes the effects of both the pressure and unburned gas temperature, they treat these effects separately:

$$S_u(T_u) = a_1 + a_2 T_u^2 \quad (27)$$

$$S_u(p) = a_3 p^{\beta} \quad (28)$$

where a_1 and a_2 are fitted coefficients which are evaluated for various pressures, and a_3 and β are fitted coefficients which are evaluated for various unburned gas temperatures. The values of these coefficients were reported for stoichiometric mixtures. For high p and T_u, the temperature effect expressions are dominated by the T_u^2 term, which agrees closely with our values of α for stoichiometric mixtures. Westbrook and Dryer's pressure exponents for $p \geq 1$ atm ($\beta = -0.181$ for $T_u = 300$ K and $\beta = -0.114$ for $T_u = 600$ K) are slightly less negative than ours. Below 1 atm, Westbrook and Dryer predict values of β roughly one third of those for $p \geq 1$ atm. Tsatsronis' pressure exponent changes significantly between 0.6 and 4 atm, which lie within our testing conditions, and so it is hard to compare with our value. He predicts the following values of β for $T_u = 298$ K: $\beta = -0.12$ for $p < 0.6$ atm and $\beta = -0.51$ for $p > 4$ atm.

Westbrook and Dryer also predict S_u (but not β) for equivalence ratios between 0.8 and 1.5, an unburned gas temperature of 300 K, and pressures of 0.1, 1, and 10 atm. S_u is predicted to be less sensitive to pressure at the higher equivalence ratios, but the pressure exponent does not become positive, as we have found.

EFFECT OF DILUENT - The addition of an N_2-CO_2 diluent reduces the adiabatic flame temperature of indolene-air mixtures much the same as does the addition of excess air (i.e. $\phi < 1$). The amount of added diluent can be expressed in terms of a heat capacity ratio, η, which is defined as the ratio of the heat capacity of the added material to the heat capacity of the combustion products of the undiluted fraction of the mixture:

$$\eta_{\text{excess air}} = 0.84 \frac{1 - \phi}{\phi} \quad (29)$$

$$\eta_{\text{diluent}} = 0.96 \frac{f_D}{1 - f_D} \quad (30)$$

Figure 12 shows that the reduction in S_u for given values of T_u and p due to the addition of diluent is much greater than the reduction due to the addition of excess air. The oxygen in the excess air helps combustion, whereas the N_2-CO_2 diluent just absorbs energy and impedes the diffusion of chemical species and heat.

CELLULAR FLAMES - Theoretical studies (16,17,18) predict that, under certain circumstances, smooth laminar flames in premixed gases develop instabilities which cause the flame front to become cellular. This may be caused either by instabilities in the fluid flow near the flame, or by an imbalance between the thermal conductivity of the mixture and the mass diffusivities of the various components in the mixture. The values of S_u presented in this study are calculated by dividing the volume rate at which the unburned gas burns by the flame area. The flame is assumed to be smooth, spherical, and completely symmetric. If the flame becomes cellular, then the area increases, and the temperatures, molecular concentrations, and flow field are no longer uniform for all sections of the flame, so the validity of the assumptions stated above must be evaluated.

Cellular flame structure has recently been photographed in lean, stoichiometric, and rich mixtures of propane-air and hydrogen-oxygen-nitrogen by Groff (19), Gussak et al. (20), and Mitani and Williams (21). Groff performed his tests in an approximately spherical combustion bomb with an inside diameter of 260 mm. His photographs are difficult to interpret because by the time the cellular structure appears, the edge of the flame is outside the field of view, so it is impossible to determine how deep the crevices are. Gussak et al. used a cylindrical combustion bomb with a diameter and height of only 16 mm. Their photographs indicate that the cellular structure significantly increases the area of the flame front. Cells start to form right from the time of the spark, whereas in Groff's photographs, cells do not appear until the radius of the flame reaches at least half the radius of the chamber.

Further work needs to be done to evaluate when laminar flames become cellular, and what effect this has on the laminar burning speeds obtained from combustion bomb experiments.

CONCLUSIONS

Based on the results of tests made on mixtures of two multi-component fuels similar to automotive gasoline with air and an N_2-CO_2 simulated residual gas, and on comparison with other work, it is concluded that:

1. The laminar burning speeds of these mixtures can be fitted to an expression of the form

$$S_u = S_{uo} \left(\frac{T_u}{T_o}\right)^{\alpha} \left(\frac{P}{P_o}\right)^{\beta} (1 - 2.06\, f_D^{0.733}) \quad (31)$$

2. Laminar burning speeds of the two multicomponent fuels peak at $\phi = 1.2$.
3. The exponents α and β are approximately independent of fuel type but are functions of ϕ. β is positive for $\phi > 1.4$ and negative for $\phi < 1.4$.

4. Laminar burning speed is reduced more by the addition of N_2-CO_2 diluent than by excess air.
5. The fractional reduction in laminar burning speed by the addition of N_2-CO_2 diluent is independent of equivalence ratio, pressure, and temperature for RMFD 303 mixtures with $0.7 \leq \phi \leq 1.2$ and this fractional reduction is roughly the same as that obtained for stoichiometric mixtures of five other fuels (12).

ACKNOWLEDGEMENT

This research was supported by the Ford Motor Company and by a Shell Companies Foundation grant.

REFERENCES

1. N.S. Blizard and J.C. Keck, "Experimental and Theoretical Investigation of Turbulent Burning Model for Internal Combustion Engines", SAE Paper 740191 (1974).

2. R.J. Tabaczynski, F.H. Trinker, and B.A.S. Shannan, Combustion and Flame, 39:111 (1980).

3. P.A. Libby and K.N.C. Bray, "Implications of the Laminar Flamelet Model in Premixed Turbulent Combustion", Combustion and Flame, 39:33-41 (1980).

4. C.R. Ferguson and J.C. Keck, "On Laminar Flame Quenching and Its Application to Spark Ignition Engines", Combustion and Flame, 28:197-205 (1977).

5. C.R. Ferguson and J.C. Keck, "Stand-Off Distances on a Flat Flame Burner", Combustion and Flame, 34:85-98 (1979).

6. J.M. Heimeri and T.P. Coffee, "The Detailed Modeling of Premixed, Laminar Steady-State Flames. I. Ozone", Combustion and Flame, 39:301-315 (1980).

7. L.D. Smoot, W.C. Hecker, and G.A. Williams, "Prediction of Propagating Methane-Air Flames", Combustion and Flame, 26:323-342 (1976).

8. G. Tsatsaronis, "Prediction of Propagating Laminar Flames in Methane, Oxygen, Nitrogen Mixtures", Combustion and Flame, 33:217-239 (1978).

9. C.K. Westbrook and F.L. Dryer, "Prediction of Laminar Flame Properties of Methanol-Air Mixtures", Combustion and Flame, 37:171-192 (1980).

10. M. Metghalchi and J.C. Keck, "Laminar Burning Velocity of Propane-Air Mixtures at High Temperature and Pressure", Combustion and Flame, 38: 143-154 (1980).

11. M. Metghalchi and J.C. Keck, "Burning Velocities of Mixtures of Air with Methanol, Isooctane, and Indolene at High Pressure and Temperature", Combustion and Flame, 48:191-210 (1982).

12. T.W. Ryan III and S.S. Lestz, "The Laminar Burning Velocity of Isooctane, N-Heptane, Methanol, Methane, and Propane at Elevated Temperature and Pressures in the Presence of a Diluent", SAE Paper 800103 (1980).

13. M.K. Martin and J.C. Heywood, "Approximate Relationships for the Thermodynamic Properties of Hydrocarbon-Air Combustion Products", Combustion Science and Technology, 15:1-10 (1977).

14. J.C. Keck, Letter in Mass and Heat Transfer, 8:313 (1981).

15. M.C. Sellnau, "Laminar Head-on Flame Quenching in a Spherical Combustion Bomb", S.M. Thesis, M.I.T., Cambridge, MA, 1981.

16. G. Joulin and T. Mitani, "Linear Stability Analysis of Two-Reactant Flames", Combustion and Flame, 40:235-246 (1981).

17. Ya.B. Zeldovich, "Structure and Stability of Steady Laminar Flame at Moderately Large Reynolds Numbers", Combustion and Flame, 40:225-234 (1981).

18. B.J. Matkowski, L.J. Putnick, and G.I. Sivashinski, "A Nonlinear Theory of Cellular Flames", SIAM Journal of Applied Mathematics, 38(3):489-504 (June, 1980).

19. E.G. Groff, "The Cellular Nature of Confined Spherical Propane-Air Flames", Research Publication, GMR-3522, General Motors Research Laboratories, Warren, MI, presented at 1981 Spring Technical Meeting, Central Section of the Combustion Institute, March, 1981.

20. L.A. Gussak, A.G. Istratov, V.B. Librovich, and E.N. Spirintsina, "Development of Perturbations at the Surface of a Flame Propagating from a Central Point Ignition Source in a Closed Vessel", Combustion, Explosion, and Shock Waves, 13(1):19-24 (Jan - Feb, 1977).

21. T. Mitani and F.A. Williams, "Studies of Cellular Flames in Hydrogen-Oxygen-Nitrogen Mixtures", Combustion and Flame, 39:169-190 (1980).

APPENDIX: BALANCED PRESSURE INDICATOR

As shown in Figure 13, the balanced pressure indicator consists, from inside outwards, of the following main parts: a 25 μm thick diaphragm, two 25 μm thick shims, two grids, two large

teflon gaskets, and two housings. The diameter of the unclamped centre section of the diaphragm is 6.35 cm. The diaphragm and shims are made of type 302 cold-rolled, full-hard stainless steel, and the grids and housings are made of type 303 stainless steel. An electrode is mounted in a depression in the balance-side grid, but is insulated from the grid. The height of the electrode is adjusted so that it protrudes about 10 μm above the grid. The two housings are bolted together and the rest of the parts are clamped between them. Mating surfaces are sealed with very small amounts of RTV.

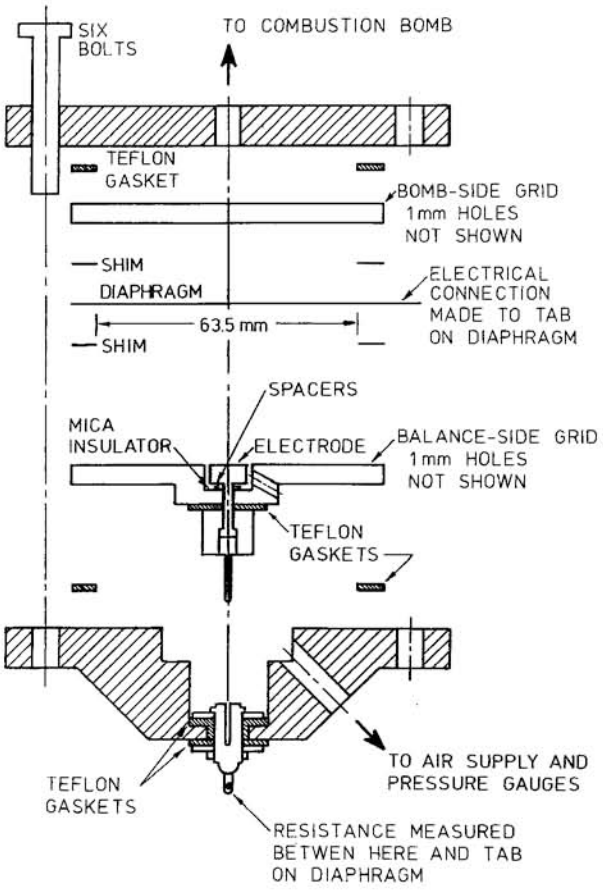

FIGURE 13: Balanced pressure indicator.

To measure the pressure inside the bomb, the balancing pressure is increased or decreased until the diaphragm just lifts off or touches the electrode. The minimum pressure difference, Δp_{min}, needed to deflect the diaphragm enough to contact the electrode is calculated (using Eq. (32) below) to be only 0.26 Pa, which is more than three orders of magnitude smaller than the minimum fuel pressure actually measured.

$$\Delta p_{min} = \frac{256}{3} \frac{Eh^3 b}{(1-\nu^2)D^4} \qquad (32)$$

where:

E = modulus of elasticity of the diaphragm
h = thickness of the diaphragm
δ = minimum deflection required for diaphragm to contact electrode
ν = Poisson's ratio
D = unsupported diameter of the diaphragm

To determine when the diaphragm first touches the electrode, the contact resistance between the diaphragm and the electrode is measured. A high sensitivity is required because the contact resistance is about $10^{11}\ \Omega$ at first contact. An alternate method would be to measure the change in capacitance between the electrode and the diaphragm.

The flow rate of balancing gas must be adjustable over a wide range, so that the balancing pressure can be increased quickly to a pressure close to the bomb pressure, and then fine-adjusted to exactly balance the bomb pressure. High flow rates are obtained using the main gas handling panel. Low flows are obtained using a gas cylinder with a sub-atmospheric pressure regulator, a small tube with a 50 μm internal diameter, a micrometering valve for flow control, and a toggle shut-off valve connected in series.

When large pressure differences are applied across the diaphragm, the centre section is pressed against one of the grids. As the pressure difference is increased, more of the diaphragm contacts the grid and the bending stresses in the unsupported region around the perimeter increase. The maximum permissible pressure difference before plastic deformation occurs is calculated to be

$$\Delta p_{max} = \frac{h(\sigma_{max})^2}{6Eb} \qquad (33)$$

where:

σ_{max} = maximum permissible stress

b = shim thickness

When the diaphragm is forced strongly against one of the grids by a large pressure difference, those unsupported sections of the diaphragm covering holes in the grid behave like miniature diaphragms. The grid holes should be small enough to prevent plastic deformation of the diaphragm near these holes. The maximum permissible grid hole diameter is calculated to be:

$$d_{max} = 0.9\ h\sqrt{\frac{\sigma_{max}}{\Delta p_{max}}} \qquad (34)$$